

# ChemComm

Accepted Manuscript



This is an *Accepted Manuscript*, which has been through the Royal Society of Chemistry peer review process and has been accepted for publication.

*Accepted Manuscripts* are published online shortly after acceptance, before technical editing, formatting and proof reading. Using this free service, authors can make their results available to the community, in citable form, before we publish the edited article. We will replace this *Accepted Manuscript* with the edited and formatted *Advance Article* as soon as it is available.

You can find more information about *Accepted Manuscripts* in the [Information for Authors](#).

Please note that technical editing may introduce minor changes to the text and/or graphics, which may alter content. The journal's standard [Terms & Conditions](#) and the [Ethical guidelines](#) still apply. In no event shall the Royal Society of Chemistry be held responsible for any errors or omissions in this *Accepted Manuscript* or any consequences arising from the use of any information it contains.

## COMMUNICATION

Cite this: DOI: 10.1039/x0xx00000x

**Bifunctional curcumin analogue for two-photon imaging and inhibiting crosslinking of amyloid beta in Alzheimer's disease**Received 00th January 2012,  
Accepted 00th January 2012Xueli Zhang<sup>1,2,5</sup>, Yanli Tian<sup>1,3,5</sup>, Peng Yuan<sup>4</sup>, Yuyan Li<sup>1,2</sup>, Mohammad A. Yaseen<sup>1</sup>,  
Jaime Grutzendler<sup>4</sup>, Anna Moore<sup>1\*</sup>, and Chongzhao Ran<sup>1\*</sup>

DOI: 10.1039/x0xx00000x

[www.rsc.org/](http://www.rsc.org/)

**In this report, we designed a highly bright bifunctional curcumin analogue CRANAD-28. *In vivo* two-photon imaging suggested that CRANAD-28 could penetrate the blood brain barrier (BBB) and label plaques and cerebral amyloid angiopathy (CAAs). We also demonstrated that this imaging probe could inhibit the crosslinking of amyloid beta induced either by copper or by natural conditions.**

An imaging probe and a drug could share a common structural scaffold and design concept considering that they have the same target<sup>1,2</sup>. They could also have similar interaction mechanisms and specificity requirements for the target. In traditional approaches, imaging probes and drugs are pursued separately, which are time-consuming and costly<sup>3,4</sup>. To overcome this disadvantage, developing agents that have potentials for therapy and imaging (theranostic) is highly desirable. Nanoparticle-based theranostics have been intensively explored<sup>4</sup>; however their poor BBB penetration limits their applications for CNS diseases. Therefore, developing small molecule-based theranostics is warranted for neurodegenerative diseases such as Alzheimer's disease<sup>2</sup> (AD).

Amyloid beta (A $\beta$ ), a peptide of 40 or 42 amino acids, is one of the key players in AD pathology<sup>5</sup>. The presence of A $\beta$  plaques is one of the hallmarks of AD<sup>5,6</sup>. **While the degree of toxicity of amyloid plaques that contribute to the overall cognitive decline in AD remains unknown**, plaques are clear sites of pathology as evidenced by the presence of dystrophic neurites and the loss of dendritic spines in their surroundings<sup>7,8</sup>. Furthermore, there is also some evidence that plaques may impair mitochondria function and calcium homeostasis and lead to cell death<sup>9</sup>. Given these and other lines of evidence, reducing A $\beta$  deposits and plaques remains an important aim for AD drug development<sup>5,10,11</sup>. Imaging probes for A $\beta$ s for both clinical and preclinical research have been reported<sup>10,12-15</sup>. However, small molecules that can be used both for imaging and therapy of AD are still urgently needed<sup>11</sup>.

Recently, we have developed curcumin analogues for detecting soluble and insoluble A $\beta$ s *in vitro*, and some of them have been successfully applied for *in vivo* near-infrared imaging in

transgenic AD mice<sup>16-18</sup>. Based on the limited interaction mechanism of the curcumin ligands and A $\beta$ s, we also designed imidazole-containing curcumin analogues to specifically interrupt the crosslinking of A $\beta$ s that was initialized by metal ions such as copper<sup>19,20</sup>. However, curcumin compounds always have low quantum yield (QY), and lack theranostic properties. In this report, we designed, synthesized and tested a bifunctional compound with high brightness for two-photon imaging and potential therapy.

To overcome the low QY limitation of curcumin analogues, we hypothesized that replacing the phenyl rings with pyrazoles could increase the brightness. Conceivably, the inductive electron-withdrawing effect of one of the nitrogens of pyrazole could lead to a low tendency of electron delocalization in the system, which will decrease tautomerization of the designed compounds. It is well known that less tautomerization can reduce non-radiative decay from the excited states, thus increase the QY<sup>21</sup>. On the other hand, in our previous studies<sup>17</sup>, we showed that imidazole containing curcumin analogues could specifically interfere the coordination of copper with H13 and H14 (Histidine) and thus attenuate the crosslinking of A $\beta$ . In this report, we speculated that pyrazole could also interfere the coordination because pyrazole can coordinate with copper as well. In addition, we reasoned that phenyl substitution at the N-1 position of pyrazole could further improve the QY due to the reduction of tautomerization of pyrazole (more tautomers, more non-radiative decay)<sup>22</sup>. Taking all the facts into consideration, CRANAD-28 was designed and synthesized (Fig.1b).

CRANAD-28, an orange powder, was synthesized following our previously published procedures<sup>16,17</sup>. We first investigated its fluorescence properties such as excitation and emission, and QY. The excitation peak of CRANAD-28 is 498 nm and the emission peak is 578 nm in PBS (Fig.1d). The Stokes shift of CRANAD-28 is considerably large (80 nm), which is highly beneficial for two-photon imaging because it provides better emission penetration due to the large Stokes shift. As we expected, CRANAD-28 has a very high QY both in PBS and ethanol. The QY of CRANAD-28 is 0.32 in PBS and > 1.0 in ethanol (rhodamine B was used as a reference). Our results are consistent with several references, which showed that pyrazoles are very important moieties contributing to strong fluorescence<sup>23-25</sup>. To confirm the N-1 phenyl substitution effect, we

also synthesized CRANAD-44. As expected, the QY of CRANAD-28 was higher than that of CRANAD-44 (QY = 0.29 in PBS and 0.47 in ethanol), because the N-1 phenyl substitution can reduce the number of annular tautomers<sup>22</sup>, and thus reduce the non-radiative emission decay (Fig.1b).

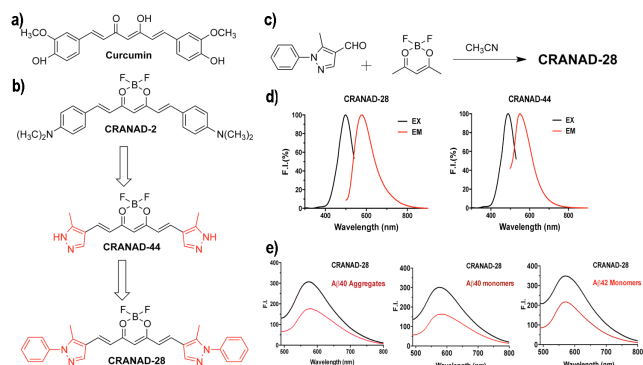


**Fig.1** a) Structure of Curcumin. b) Design of CRANAD-28 through pyrazole replacement. c) The synthetic route for CRANAD-28. d) The excitation/emission spectra of CRANAD-28 and -44. e) Fluorescence responses of CRANAD-28 with A $\beta$ 40 aggregates, A $\beta$ 40 monomers and A $\beta$ 42 monomers. For A $\beta$ 42 dimers and oligomers, the spectra are shown in SI Fig.1.

To test whether CRANAD-28 could interact with various A $\beta$ s, we first incubated the compound with soluble A $\beta$ s that included monomeric, dimeric, and oligomeric A $\beta$ s. We also tested the compound with insoluble A $\beta$ 40 aggregates. Interestingly, we observed that the fluorescence intensity of CRANAD-28 decreased upon mixing with all of the tested A $\beta$ s, indicating that CRANAD-28 could interact with these A $\beta$ s (Fig.1e and SI Fig.1). The K<sub>d</sub> values of CRANAD-28 with A $\beta$ 40 monomers, A $\beta$ 42 monomers, A $\beta$ 42 dimers, A $\beta$ 42 oligomers, and A $\beta$ 40 aggregates were 68.8, 159.7, 162.9, 85.7 and 52.4 nM, respectively (SI Fig.1b) (see details of K<sub>d</sub> measurement in supplemental information). The intensity decrease of CRANAD-28 is contrary to our previously reported fluorescent probes, which showed intensity increase with A $\beta$ s. No significant change was observed for CRANAD-44 with soluble A $\beta$ s (SI Fig.2b, c). It is not clear what are the quenching mechanisms for the intensity decrease of CRANAD-28. Hintersteiner et al reported that the fluorescence of imaging probe AOI987 could be slightly quenched by A $\beta$  aggregates through an unknown mechanism<sup>26</sup>, and Chen et al showed that Alexa fluorophores could be quenched by amino acids such as histidine, tyrosine, and methionine through static and collisional mechanisms<sup>27</sup>. Other mechanisms that include electron-scavenging<sup>28</sup> and photoinduced electron transfer (PeT)<sup>29</sup> were also proposed for the quenching effect induced by peptides and amino acids<sup>30</sup>. The fluorescence quenching of CRANAD-28 by A $\beta$ s could be due to one or a combination of the above mechanisms.

To further test whether the compounds could label A $\beta$  plaques in AD brain tissue, we stained APP/PS1 mouse brain slices with CRANAD-28 and -44. Thioflavin S, a standard plaque-staining agent, was used for staining consecutive slices. We found that CRANAD-28 could provide excellent contrast for A $\beta$  plaques (Fig.2a-c), and the distribution pattern of the highlighted plaques was similar to that with Thioflavin S staining. However, CRANAD-44 did not show obvious contrast for plaques, suggesting that the phenyl rings at the N-1 position could enhance the binding with A $\beta$ s (Fig.2 and SI Fig.3). Meanwhile, CRANAD-28 not only stained the

plaques, but also labeled CAAs (Fig.2d, e), which is characterized by A $\beta$  deposits at the exterior of the brain blood vessels that significantly contribute to pathological dementia<sup>31</sup>.

To investigate whether CRANAD-28 could be used for *in vivo* two-photon imaging of A $\beta$  plaques, we firstly examined its BBB penetration. To this end, CRANAD-28 was injected i.v. into a wild type mouse, which had a surgically induced thinned skull<sup>32-34</sup>. We quantified the BBB penetration following the reported method<sup>35</sup>, and found that CRANAD-28 reached its peak around 5 minutes after injection, followed by a slow wash out (SI Fig.4). Since CRANAD-44 was not able to label A $\beta$  plaques in the brain tissue, we didn't test BBB penetration of this compound.

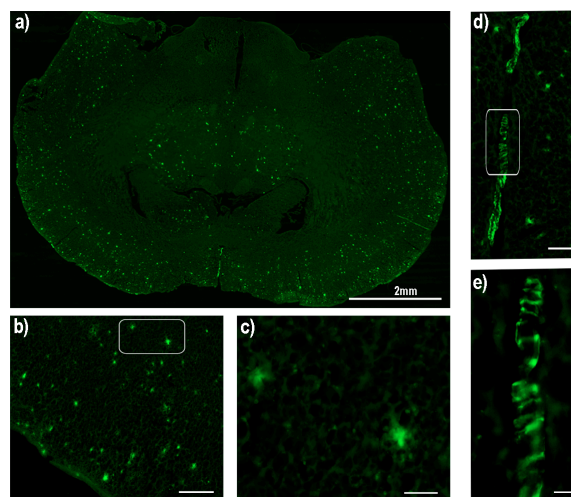


**Fig.2** Histological staining of a brain slice of an APP/PS1 mouse with CRANAD-28. a) The image of the whole slice (2x). b) Image of the cortex area (10x) (scale bar: 200 micron), and c) Image of two plaques in the white box in b (40x) (scale bar: 100 micron). d) Image of CAAs (10x) (scale bar: 200 micron), and e) Magnified image of white box in d (40x) (scale bar: 100 micron).

Next, to validate the capability of CRANAD-28 for *in vivo* two-photon imaging of A $\beta$  plaques, we used 9-month old APP/PS1 mice that had thinning skull surgery<sup>32-34</sup>. This procedure is significantly less invasive compared to cranial window preparation, which requires total removal of the skull<sup>36,37</sup>. In addition, it causes less damage to the neuronal cells and therefore is preferable<sup>37</sup>. After i.v. injection of CRANAD-28, CAAs were clearly highlighted around the imaged vessels (Fig.3a, white arrowhead). As expected, A $\beta$  plaques could also be clearly labeled (Fig.3a, yellow arrowhead). In Fig.3, the blood vessels were highlighted by the injected Texas-red dextran (70,000 MW). There was a clear localization of CAAs on the wall of the vessels. These results suggested that CRANAD-28 was an effective two-photon imaging probe for both CAA and A $\beta$  plaques. Moreover, the data also demonstrated that the longer emission of CRANAD-28 could allow for imaging to be performed with a less invasive thinning skull surgery<sup>32-34</sup>.

For a specific target, a non-tagged imaging probe could serve both as a ligand and a fluorophore. Conceivably, such probe could engage with the target, and thus affect the behavior of the target. For A $\beta$  species, CRANAD-28 could also have the capacity to change its folding/aggregating behavior, and thus to execute its anti-crosslinking effect. In our previous studies, we have demonstrated that the imidazole-containing curcumin analogue CRANAD-17

could specifically interrupt the copper induced crosslinking of A $\beta$ , due to the imidazole moiety, which could interfere with the copper coordination with H13 and H14 of A $\beta$ <sup>17</sup>. In CRANAD-28, the pyrazole ring could have the capability to coordinate with copper<sup>38</sup>, and thus may have the ability to compete with H13/H14 coordination. Therefore, it is reasonable to speculate that CRANAD-28 can also attenuate copper-induced crosslinking of A $\beta$ . To this end, we first tested CRANAD-28 with FAM-A $\beta$ 42, a dye (FAM) conjugated A $\beta$ 42, to investigate the anti-crosslinking effect. As expected, there was significantly more (4.13-fold) monomeric A $\beta$  remaining in CRANAD-28 treated samples than that in the control samples, indicating reduced crosslinking (Fig.4a). To further investigate whether it could inhibit the crosslinking of native A $\beta$ 42, we used western blotting to quantify the remaining A $\beta$  momomers. Similar to the result with FAM-A $\beta$ 42, CRANAD-28 treatment resulted in considerably more monomeric A $\beta$  free of crosslinking (1.85-fold) (Fig.4b).

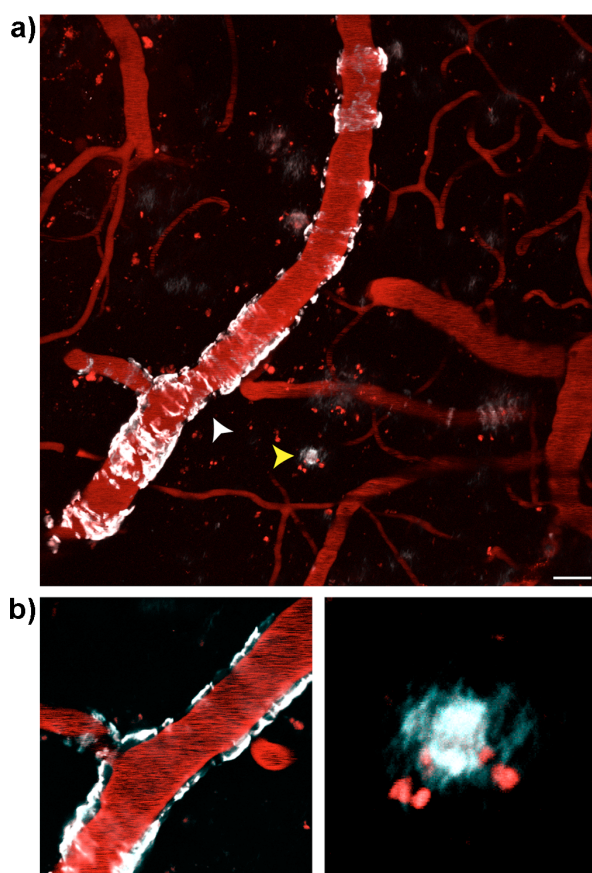


**Fig.3** Two-photon *in vivo* images of CRANAD-28 labeling in a 9-month-old APP/PS1 mouse. (a) Images were taken through a thinned-skull window 15min after i.v. infusion of the dye. Both CAA and amyloid plaques were labeled with CRANAD-28. (b) Lower panels show zoomed-in single focal plane examples of CAA (white arrowhead, left panel) and amyloid plaque (yellow arrowhead, right panel). Blood vessels were labeled with Texas-red dextran (70,000 MW). Red punctate signals are auto-fluorescence intracellular structures. Scale bar: 25  $\mu$  m.

Besides induction by metal ions, crosslinking of A $\beta$ 42 can occur naturally in solution, which is also an important factor contributing to its toxicity. To investigate whether CRANAD-28 could attenuate the natural crosslinking, we incubated it with A $\beta$ 42

in PBS buffer for 24 hours. Western blotting analysis showed that CRANAD-28 could significantly inhibit natural crosslinking of A $\beta$ 42 (2.89-fold higher than the control) (Fig.4c).

To investigate whether the compounds' A $\beta$ -specificity has any effects on anti-crosslinking induced by copper and a natural condition, we compared the monomeric bands of CRANAD-28 and CRANAD-44 on western blotting, and found that CRANAD-44 was not efficient in inhibiting the crosslinking of A $\beta$ 42 under both conditions (Fig.4b,c). This is consistent with our fluorescence studies and histological staining, which indicated that CRANAD-44 was not A $\beta$ -specific.

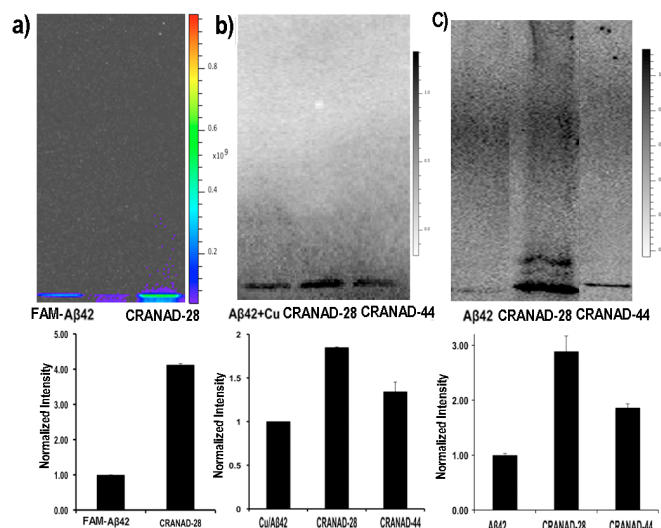


**Fig.4** Anti-crosslinking effect of CRANAD-28. a-c) SDS-PAGE gel with FAM-A $\beta$ 42 treated with copper (a), western blot of native A $\beta$ 42 treated with copper (b) and western blotting of native A $\beta$ 42 under natural conditions (c) (up panel). Bottom panel: quantitative analysis of the monomeric bands for each condition in the upper panel (n=4). The normalization was based on FAM-A $\beta$ 42 treated with copper (a), A $\beta$ 42 treated with copper (b), and A $\beta$ 42 only (c).

In summary, we demonstrated that CRANAD-28 could be considered a theranostic agent due to its imaging and potential therapeutic functions. Through replacement of the phenyl rings with pyrazole, the resulting CRANAD-28 displayed high QY in PBS and ethanol. Previously, analogues of PiB, styrybenzene, and other compounds have been reported to be very reliable imaging probes for two-photon imaging<sup>35, 39, 40</sup>. However, due to their short emission wavelengths, these dyes are associated with poor tissue penetrating capacities. Conceivably, CRANAD-28 has better tissue penetration because of its longer emission. Multi-color time-stamp has been considered to be a very useful tool to investigate the growth kinetics of plaques, and this technique can provide comprehensive toxicity profile of plaques<sup>8</sup>. We believe that fluorescent dyes with longer emissions, like CRANAD-28, could be very useful for sequential multi-color labeling to avoid *ex vivo* section staining. In addition, CRANAD-28 is not only useful for two-photon imaging but also has the capacity to attenuate crosslinking of A $\beta$ 42 induced by metal ion and natural conditions. We believe that its bifunction could contribute to AD diagnosis and therapy development in the future.

**Acknowledgement.** This work was supported by K25AG036760 award to C.R and K99AG042026 award to M.A.Y. The authors

would also like to thank Pamela Pantazopoulos, B.S. for proofreading this manuscript.

## Notes

1. Molecular Imaging Laboratory, A. A. Martinos Center for Biomedical Imaging, Massachusetts General Hospital/Harvard Medical School, Building 75, Charlestown, Massachusetts 02129;
2. School of Pharmacy, China Pharmaceutical University, Nanjing, China;
3. Department of Parasitology, Zhongshan School of Medicine, Sun Yat-Sen University, Guangzhou, China;
4. Department of Neurology, Yale University, New Haven, CT;
5. These authors contributed equally to this work.

**Corresponding author email:** cran@nmr.mgh.harvard.edu and amooore@helix.mgh.harvard.edu

Electronic Supplementary Information (ESI) available: [synthesis and detailed experimental procedures]. See DOI: 10.1039/c000000x/

## References

1. S. Vallabhajosula, *Molecular imaging : radiopharmaceuticals for PET and SPECT*, Springer-Verlag, Berlin ; New York, 2009.
2. S. Aulic, M. L. Bolognesi and G. Legname, *Int J Cell Biol*, 2013, **2013**, 150952.
3. A. de la Zerda, J. W. Kim, E. I. Galanzha, S. S. Gambhir and V. P. Zharov, *Contrast Media Mol Imaging*, 2011, **6**, 346-369.
4. J. Xie, S. Lee and X. Chen, *Adv Drug Deliv Rev*, 2010, **62**, 1064-1079.
5. D. J. Selkoe, *Nat Med*, 2011, **17**, 1060-1065.
6. C. L. Joachim, H. Mori and D. J. Selkoe, *Nature*, 1989, **341**, 226-230.
7. J. Tsai, J. Grutzendler, K. Duff and W. B. Gan, *Nat Neurosci*, 2004, **7**, 1181-1183.
8. C. Condello, A. Schain and J. Grutzendler, *Sci Rep*, 2011, **1**, 19.
9. H. Xie, J. Guan, L. A. Borrelli, J. Xu, A. Serrano-Pozo and B. J. Bacskai, *J Neurosci*, 2013, **33**, 17042-17051.
10. R. Jakob-Roetne and H. Jacobsen, *Angew Chem*, 2009, **48**, 3030-3059.
11. W. Yang, Y. Wong, O. T. Ng, L. P. Bai, D. W. Kwong, Y. Ke, Z. H. Jiang, H. W. Li, K. K. Yung and M. S. Wong, *Angew Chem*, 2012, **51**, 1804-1810.
12. M. Ono, Watanabe, H., Kimura, H., Saji, H., *ACS Chem. Neurosci.*, 2012, **3**, 319-324.
13. M. Cui, M. Ono, H. Watanabe, H. Kimura, B. Liu and H. Saji, *J Amer Chem Soc*, 2014, **136**, 3388-3394.
14. N. P. Cook, M. Ozbil, C. Katsampes, R. Prabhakar and A. A. Marti, *J Amer Chem Soc*, 2013, **135**, 10810-10816.
15. C. Ran, Zhao, W., Moir, RD, Moore, A. , *PLoS One*, 2011, **6**, e19362.
16. C. Ran, X. Xu, S. B. Raymond, B. J. Ferrara, K. Neal, B. J. Bacskai, Z. Medarova and A. Moore, *J Am Chem Soc*, 2009, **131**, 15257-15261.

17. X. Zhang, Y. Tian, Z. Li, X. Tian, H. Sun, H. Liu, A. Moore and C. Ran, *J Amer Chem Soc*, 2013, **135**, 16397-16409.
18. C. Ran and A. Moore, *Molecular Imaging Biol*, 2012, **14**, 293-300.
19. C. S. Atwood, G. Perry, H. Zeng, Y. Kato, W. D. Jones, K. Q. Ling, X. Huang, R. D. Moir, D. Wang, L. M. Sayre, M. A. Smith, S. G. Chen and A. I. Bush, *Biochemistry*, 2004, **43**, 560-568.
20. G. Thiabaud, S. Pizzocaro, R. Garcia-Serres, J. M. Latour, E. Monzani and L. Casella, *Angew Chem*, 2013, **52**, 8041-8044.
21. J. Lakowicz, *Principles of Fluorescence Spectroscopy*, 2nd edition edn., Plenum Publishing Corporation, 1999.
22. J. de Paz, J. Elguero, C. Foces-Foces, A. Llamas-Saiz, F. Aguilar-Parrilla, O. Klein and H. Limbach, *J. Chem. Soc., Perkin Trans. 2*, 1997, 101-109.
23. W. Song, Y. Wang, J. Qu, M. M. Madden and Q. Lin, *Angew Chem*, 2008, **47**, 2832-2835.
24. Z. Yu, L. Y. Ho and Q. Lin, *J Amer Chem Soc*, 2011, **133**, 11912-11915.
25. T. Ren, H. Cheng, J. Zhang, W. Li, J. Guo and L. Yang, *J. Fluoresc*, 2012, **22**, 201-212.
26. M. Hintersteiner, A. Enz, P. Frey, A. L. Jatton, W. Kinzy, R. Kneuer, U. Neumann, M. Rudin, M. Staufenbiel, M. Stoeckli, K. H. Wiederhold and H. U. Gremlich, *Nat Biotechnol*, 2005, **23**, 577-583.
27. H. Chen, S. S. Ahsan, M. B. Santiago-Berrios, H. D. Abruna and W. W. Webb, *J Amer Chem Soc*, 2010, **132**, 7244-7245.
28. M. R. Eftink and C. A. Ghiron, *Anal Biochem*, 1981, **114**, 199-227.
29. G. Bottari, G. de la Torre, D. M. Guldi and T. Torres, *Chem Rev*, 2010, **110**, 6768-6816.
30. M. Sauer and H. Neuweiler, *Methods Mol Biol*, 2014, **1076**, 597-615.
31. E. E. Smith and S. M. Greenberg, *Stroke*, 2009, **40**, 2601-2606.
32. J. Grutzendler, N. Kasthuri and W. B. Gan, *Nature*, 2002, **420**, 812-816.
33. J. Grutzendler, G. Yang, F. Pan, C. N. Parkhurst and W. B. Gan, *Cold Spring Harb Protoc*, 2011, **2011**.
34. D. F. Marker, M. E. Tremblay, S. M. Lu, A. K. Majewska and H. A. Gelbard, *JoVE*, 2010, pii: 2059.
35. B. J. Bacskai, G. A. Hickey, J. Skoch, S. T. Kajdasz, Y. Wang, G. F. Huang, C. A. Mathis, W. E. Klunk and B. T. Hyman, *Proc Natl Acad Sci U S A*, 2003, **100**, 12462-12467.
36. R. Mostany and C. Portera-Cailliau, *JoVE*, 2008, pii: 680
37. H. T. Xu, F. Pan, G. Yang and W. B. Gan, *Nat Neurosci*, 2007, **10**, 549-551.
38. T. Otieno, J. Blanton, M. Hatfield, S. Asher and S. Parkin, *Acta Crystallogr C.*, 2002, **58**, m182-185.
39. E. E. Nesterov, J. Skoch, B. T. Hyman, W. E. Klunk, B. J. Bacskai and T. M. Swager, *Angew Chem*, 2005, **44**, 5452-5456.
40. Z. Liu, C. Condello, A. Schain, R. Harb and J. Grutzendler, *J Neurosci*, 2010, **30**, 17091-17101.